Ocean Engineering 101 (2015) 118–130

Contents lists available at ScienceDirect

Ocean Engineering

journal homepage: www.elsevier.com/locate/oceaneng

Cnoidal wave induced seabed response around a buried pipeline

Xiang-Lian Zhou [a,b,*], Jun Zhang [a,b], Jun-Jie Guo [b], Jian-Hua Wang [b], Dong-Sheng Jeng [b,c]

[a] State Key Laboratory of Ocean Engineering, Shanghai Jiao Tong University, Shanghai 200240, China
[b] Centre for Marine Geotechnical Engineering, Shanghai Jiao Tong University, Shanghai 200240, China
[c] Griffith School of Engineering, Griffith University Gold Coast Campus, Queensland QLD 4222, Australia

ARTICLE INFO

Article history:
Received 9 May 2014
Accepted 4 April 2015

Keywords:
Cnoidal wave
Porous seabed
Pipeline
Liquefaction

ABSTRACT

The evaluation of wave-induced pore pressures and effective stresses in a poroelastic seabed is important for coastal and ocean engineers in the design of marine structures. Most previous theoretical investigations have focused commonly on the Stokes wave induced seabed response. In this paper, a cnoidal wave–seabed–pipeline system is modeled using the finite element method. Taylor's expression and the precise integration method are used to estimate the Jacobian elliptic function. The seabed is treated as a poroelastic medium and is characterized by Biot's partly dynamic equations (u–p model). The pore water pressure and effective vertical stress on the poroelastic seabed around a buried pipeline are examined. Based on the numerical results, a parametric study is conducted to examine the effects of wave and seabed characteristics on the seabed response. Comparison with the cnodial wave and Stokes wave induced seabed response is also demonstrated here. It implies that the difference between the maximum pore pressure and vertical effective stress induced by the cnoidal wave and Stokes wave may reach 60–70%.

1. Introduction

Submarine pipelines have been used extensively to transport offshore oil, gas and hydrocarbon resources from the bottom of the ocean floor to land. A convenient wave model in coastal and ocean engineering is that of a periodic wave propagating steadily without any change of profile in water of constant depth. There are two main wave theories for solving this problem accurately. The first is to use Stokes theory, which is based on Fourier representation of the wave, and is most suitable for waves which are not very long relative to the water depth. The second approach, better suited to shallow water, is to use a cnoidal theory, in which the Jacobian elliptic function is used, and which is based on an assumption that the water depth is less than about 1/10 of the wavelength (Wiegel, 1960). The cnoidal wave is the most important loading controlling the hydrodynamic behavior. However, especially the stability and liquefaction phenomenon of the seabed induced by cnoidal waves has not yet been clearly addressed in ocean engineering, one reason being unfamiliarity with estimating the Jacobian elliptic function.

Based on different methods, the cnoidal water wave formula can be calculated. Methods include the use of power series, Fourier series, θ function and Landen transformations. Among these, Fenton and Gardiner-Garden (1982) gave an alternative expression for elliptic functions by using the imaginary transformation, which converges most rapidly in the limit where previously presented expressions do not converge. Wiegel (1960) studied the first-order cnoidal wave. As well as results for the celerity and shape of wave and local acceleration fields, expressions and graphs for water particle velocity were given. Isobe (1985) obtained the solutions of the first-order cnoidal wave in terms of power series of theta functions, but the graphs can only give rough results and the theta functions are too complex for practical engineering. Synolakis et al. (1988) studied the maximum relative run-up of cnoidal waves climbing up a plane beach. The results showed that the maximum relative run-up of a cnoidal wave is significantly larger than the run-up of a monochromatic wave with the same wave height and wavelength far from the shore. Cho (2003) presented a numerical algorithm to calculate the Jacobian elliptic parameter by using the Newton–Raphson method. The proposed algorithm can be used to calculate cnoidal waves.

Moreover, based on different assumptions of the rigidity of the soil skeleton and the compressibility of pore fluid, numerous theories have been developed for the wave-induced soil response (Yamamoto et al., 1978; Madsen, 1978; Zienkiewicz et al., 1980; Mei and Foda, 1981; Cheng and Liu, 1986; Hsu et al., 1995; Magda, 1997; Yuhi and Ishida, 1998; Jeng and Cha, 2003; Cai et al., 2007; Liu and Jeng, 2007; Ulker and Rahman, 2009; Xu and Dong, 2011; Zhou et al., 2011; Zhang et al., 2013; Jeng, 2013; Ye et al., 2014). Among these, Mei and Foda (1981) investigated the boundary-layer approximation method

* Corresponding author at: State Key Laboratory of Ocean Engineering, Shanghai Jiao Tong University, Shanghai 200240, China. Tel.: +86 21 3420 4833; fax: +86 21 3420 4833.
E-mail addresses: zhouxl99@hotmail.com, zhouxl@sjtu.edu.cn (X.-L. Zhou).

http://dx.doi.org/10.1016/j.oceaneng.2015.04.032
0029-8018/

for the wave-induced soil response. However, the boundary-layer approximation has been proved to be limited to a seabed of fine sand (Hsu and Jeng, 1994). Based on Mei and Foda's (1981) model, Yuhi and Ishida (1998) obtained an analytical solution for the wave-induced seabed response, which directly solves the boundary value problem, rather than using the boundary layer approximations. Liu and Jeng (2007) further proposed a simple semi-analytical model for a random wave-induced soil response for an unsaturated sandy seabed of finite thickness, which may be the only analytical solution for the random wave-induced soil response. Zhou et al. (2011) used the Transmission and Reflection Matrices (TRM) method to solve the wave-induced seabed response in a multi-layered poroelastic seabed.

Similarly, the wave-induced response around a pipeline has also been studied by numerous researchers (McDougal et al., 1988; Sumer and Fredsøe, 1991; Jeng and Cheng, 2000; Sumer et al., 2001; Wang et al., 2011; Gao et al., 2011, 2012; Zhou et al., 2013, 2014). Cheng and Liu (1986) considered a buried pipeline in a region that is surrounded by two impermeable walls. McDougal et al. (1988) developed an analytical model for estimating the pore pressure in the sandy soil and the resulting pressure force on the submarine pipelines. Sumer and Fredsøe (1991) and Sumer et al. (2001) conducted a series of experiments focusing on the stability of pipelines on a liquefied sandy seabed and the onset of scour around the pipeline. By analyzing the pore water pressures measured at the upstream and downstream of a slightly buried pipeline, they have shown that the excessive seepage flow due to the pore pressure gradient in the soil and the resulting piping are the major factors causing the onset of scour. Jeng and Cheng (2000) investigated the distribution of internal stress within a buried pipe subjected to water wave loading. Shabani and Jeng (2008) developed a three-dimensional numerical model to analyze the behavior of soil around a pipeline under wave loading by using the finite element method. Gao et al. (2002) obtained an empirical formula for the prediction of pipeline instability of both freely laid pipelines and anti-rolling pipelines, based on the analysis of a series of experimental results in an oscillatory flow tunnel. Zhou et al. (2013, 2014) investigated the wave- and current-induced isotropic and anisotropic seabed response around a submarine pipeline. The third-order solution of wave–current interactions is used to determine the dynamic pressure acting on the seabed.

The main objective of this paper is to investigate the cnoidal wave-induced seabed response with a buried pipeline and liquefaction phenomenon. The cnoidal wave theory can be solved by using Taylor series expansion and a precise integration method. Then, Biot's partly dynamic equation (u–p model) is solved by the finite element method. The effects of wave and seabed characteristics, including wave height, water depth, permeability, and degree of saturation on the seabed response, are presented. Finally, the possibility of wave-induced liquefaction occurring in the porous seabed around a pipeline is studied.

2. Water pressure on the seabed subjected to cnoidal waves

Consider the wave shown in Fig. 1, where the cnoidal water wave level located at $z=-d$ is travelling along the positive x-direction, and assume the vertical z-axis is downward from the surface of the seabed (water–soil interface, $z=0$). The free water surface profile of the first-order cnoidal wave can be written as (Korteweg and De Vries, 1895; Mei et al., 2005)

$$\eta = H\left(\frac{1}{m^2}-1-\frac{E}{m^2K}\right)+Hcn^2\left[2K\left(\frac{x}{L}-\frac{t}{T}\right)\right] \tag{1}$$

where H is the wave height; $cn(\,)$ is the cnoidal function; x is the horizontal coordinate; L is the wave length, $L=4Kmd\sqrt{d/3H}$; T is the wave period; m is a parameter related to the Ursell

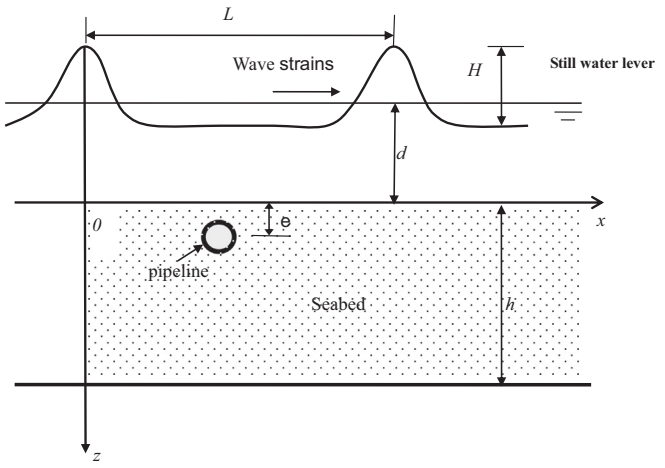

Fig. 1. Sketch of cnoidal wave–pipeline–seabed.

number; K and E are the first and second kind of complete elliptic integral, respectively, and can be expressed as

$$E=\int_0^{\frac{\pi}{2}}\sqrt{1-m^2\sin^2\varphi}\,d\varphi \tag{2}$$

$$K=\int_0^{\frac{\pi}{2}}\frac{1}{\sqrt{1-m^2\sin^2\varphi}}d\varphi \tag{3}$$

Solving the cnoidal wave problem is done by evaluating the Jacobian elliptic parameter m, elliptic integrals K and E and function cn. The most important problem is to determine m accurately because K, E and cn are all functions of m. Hedges (1995) suggested that the boundary between the application of Stokes and cnoidal theory is the Ursell number $U=40$, in which case, $m\approx 0.933$ (Fenton, 1990). This is an indication that, roughly speaking, m is always greater than 0.93 when cnoidal theory is used within its recommended limits.

Firstly, formulas of the calculation for the Jacobian elliptic parameter are studied in this section. The Taylor's expressions for the Jacobian elliptic functions at $x=0$ have the following forms (Xu et al., 2013):

$$sn(x,m)=x-\frac{1+m^2}{6}x^3+o(x^5) \tag{4}$$

$$cn(x,m)=1-\frac{1}{2}x^2+(1+4m^2)\frac{x^4}{4!}-o(x^6) \tag{5}$$

$$dn(x,m)=1-m^2\frac{1}{2}x^2+m^2(4+m^2)\frac{x^4}{4!}+o(x^6) \tag{6}$$

The elliptic functions have also the following formulas (Xu et al., 2013):

$$sn(2x,m)=\frac{2sn(x,m)cn(x,m)dn(x,m)}{1-m^2sn^4(x,m)} \tag{7}$$

$$cn(2x,m)=\frac{1-2sn^2(x,m)+m^2sn^4(x,m)}{1-m^2sn^4(x,m)}=1-\frac{2sn^2(x,m)\left[1-m^2sn^2(x,m)\right]}{1-m^2sn^4(x,m)} \tag{8}$$

$$dn(2x,m)=\frac{1-2m^2sn^2(x,m)+m^2sn^4(x,m)}{1-m^2sn^4(x,m)}=1-\frac{2m^2sn^2(x,m)\left[1-sn^2(x,m)\right]}{1-m^2sn^4(x,m)} \tag{9}$$

For convenience, we let

$$\frac{2sn^2(x,m)\left[1-m^2sn^2(x,m)\right]}{1-m^2sn^4(x,m)}=C \tag{10}$$

$$\frac{2m^2sn^2(x,m)\left[1-sn^2(x,m)\right]}{1-m^2sn^4(x,m)}=D \tag{11}$$

Moreover, Eqs. (8) and (9) can be further simplified as

$$cn(2x,m)=1-C \tag{12}$$

$$dn(2x,m)=1-D \tag{13}$$

The parameter m is evaluated as accurately as possible also because the surface profile of the cnoidal wave is highly sensitive to m. The relationships parameters of cnoidal waves can be written as (Cho, 2003)

$$HL^2=\frac{16}{3}h^3mK^2 \tag{14}$$

$$L^2=ghT^2\left[1+\frac{H}{hm}\left(2-m-3\frac{E}{K}\right)\right] \tag{15}$$

Since in laboratory applications, the specification of the wave period is more practical than specifying the wavelength, we obtain an equation for the wave period T by substituting Eq. (15) into Eq. (14) (Cho, 2003)

$$T^2=\frac{16h^3m^2K^2}{3gH\left[mh+H\left(2-m-3\frac{E}{K}\right)\right]} \tag{16}$$

Because Eq. (16) is an implicit form for m, it should be solved by the iterative numerical scheme. Eq. (16) can be rewritten as

$$Y(m)=mh+H\left(2-m-3\frac{E}{K}\right)-\frac{16}{3gHT^2}h^3mK^2 \tag{17}$$

Taking derivative of $Y(m)$ with respect to m $((dY/dm)=0)$, then, the parameter m can be estimated by using the Newton–Raphson method. Details of NR can be founded in Cho (2003) and will not be repeated here.

In this paper, the precise integration method (Zhong, 2004) can be used to reach high precision for the initial value problem. It is suggested to select $x'=(x/2^n)$ (e.g., $n=20$) to get a suitably small initial value in order to guarantee that x is a small number. Given that $cn(x,m)$ has a period of $4K$, for any $x\in(-\infty,+\infty)$, there is a corresponding number $x'(x'\le 4K)$, such that $cn(x,m)=cn(x',m)$. In the cnoidal water wave theory, $cn\left[2K\left((x/\lambda)-(t/T)\right),m\right]$ is required. For any $\left((x/\lambda)-(t/T)\right)$, we can define a variable ξ $(|\xi|\le 2)$, such that (Xu et al., 2012)

$$cn(x,m)=cn\left[2K\left(\frac{x}{\lambda}-\frac{t}{T}\right),m\right]=cn(2K\xi,m) \tag{18}$$

When considering the numerical integration based on the precise integration method, the cnoidal function $y=cn\left[2K\left((x/\lambda)-(t/T)\right),m\right]$ can be solved by the following process method:

(1) Define a variable ξ such that the initial point x is a small number;
(2) Find the number ξ which satisfies Eq. (18);
(3) Let $\zeta=\frac{2K\xi}{1024}$ and use Eqs. (4)–(6) to obtain$sn(\zeta,m)$, $cn(\zeta,m)$, $dn(\zeta,m)$;
(4) Calculate $S_1=sn(2\zeta,m)$, $C_1=\frac{2sn^2(2\zeta,m)\left[1-m^2sn^2(\zeta,m)\right]}{1-m^2sn^4(\zeta,m)}$, $D_1=\frac{2m^2sn^2(\zeta,m)\left[1-sn^2(\zeta,m)\right]}{1-m^2sn^4(\zeta,m)}$ with Eqs. (7), (10), (11);
(5) Note $2^{10}=1024$, then repeat (3) for nine times, and obtain S_{10}, C_{10}, D_{10};
(6) At least, $y=cn(2K\zeta,m)=1-C_{10}$.

3. Governing equations of porous seabed

The equations for overall equilibrium in a poroelastic medium, the relationship between effective stresses and pore pressure are given by

$$\sigma_{ij}=\sigma'_{ij}-\delta_{ij}p \tag{19}$$

where σ_{ij} and σ'_{ij} are total stress and effective stress, respectively, and are considered to be positive in tension; δ_{ij} is Kronecker delta; p is the pore pressure, which is considered to be positive in compression.

It is assumed that the seabed material can be treated as a deformable porous media with linear elastic deformation (Biot, 1956, 1962). The seabed model is based on Biot's partly dynamic theory, in which the fluid is compressible due to a small degree of unsaturation and the flow is governed by Darcy's law (Rahman et al., 1994). These assumptions can be used in the slightly unsaturated seabed where the degree of saturation is sufficiently high. The equations for the equilibrium of a porous medium and fluid are as follows (Zienkiewicz et al., 1980):

$$\sigma_{ij,j}+\rho g_i=\rho\ddot{u}_i \quad (i,j=x,z) \tag{20}$$

$$-p_{,i}+\rho_f g=\rho_f\ddot{u}_i+\frac{\rho_f g}{k_i}\dot{\overline{w}}_i \tag{21}$$

$$\dot{\varepsilon}_{ii}+\dot{\overline{w}}_{ii}=-n\beta\dot{p} \tag{22}$$

where ρg_i is the body force of the soil; u_i denotes the average solid displacement; ρ denotes the density of the porous medium; $\rho=(1-n)\rho_s+\rho_f$, ρ_s is the density of the solid skeleton, n is the soil porosity; $\overline{w}_i$ denotes the average fluid displacement relative to the solid frame, and the compressibility of pore fluid β depends on the degree of saturated S_r,$\beta$and the volume strain of soil matrix ε_{ii}:

$$\beta=\frac{1}{k_w}+\frac{1-S_r}{P_{w0}} \tag{23}$$

$$\varepsilon_{ii}=\frac{\partial u_x}{\partial x}+\frac{\partial u_z}{\partial z} \tag{24}$$

where k_w is the bulk modulus of pore water ($k_w=2\times10^9\ N/m^2$); S_r is the degree of saturation of the seabed; u_x and u_z are the soil displacements in the horizontal and vertical directions, respectively; P_{w0} is the absolute water pressure.

Substituting (21) into (22), we have

$$k_z p_{,ii}-\gamma_w n\beta\dot{p}+\rho_f\ddot{\varepsilon}_{ii}=\gamma_w\dot{\varepsilon}_i \tag{25}$$

Based on the relationship between effective stresses and displacement, the equations governing the equilibrium of a porous medium can be expressed in terms of pore pressure and soil displacements as

$$G\nabla^2u_x+\frac{G}{1-2\nu}\frac{\partial\varepsilon}{\partial x}=\frac{\partial p}{\partial x}+\rho\frac{\partial^2u_x}{\partial t^2} \tag{26}$$

$$G\nabla^2u_z+\frac{G}{1-2\nu}\frac{\partial\varepsilon}{\partial z}+\rho g=\frac{\partial p}{\partial z}+\rho\frac{\partial^2u_z}{\partial t^2} \tag{27}$$

Note that the above equations are so-called u–p approximations, which were first proposed by Zienkiewicz et al. (1980), and applied to the wave-seabed interaction problem.

4. Boundary condition

For a porous seabed of finite thickness, it is commonly accepted that the vertical effective stress and shear stress vanish. The pore pressure is equal to the wave pressure at the seabed surface:

$$\sigma'_{zz}=\sigma_{zx}=0 \tag{28}$$

$$p = p_b \quad \text{at} \quad z = 0 \tag{29}$$

In cnoidal water, the velocity in a vertical direction may be neglected and that the horizontal velocity may be consider uniform across each of vertical section in shallow water (Korteweg and De Vries, 1895), the pore pressure at the interface between the water and the porous seabed is identical to the wave pressure at the seabed surface, and the cnoidal wave pressure on the seabed surface can be written as (Wiegel, 1960)

$$p = p_b = \rho_w g \eta \tag{30}$$

The bottom of a porous seabed with finite thickness is treated as impermeable and rigid, and zero displacement and no vertical flow occurs in this bottom boundary:

$$u_x = u_z = \frac{\partial p}{\partial z} = 0 \quad \text{at} \quad z = h \tag{31}$$

Most previous studies of wave–seabed–pipeline interaction have assumed that the pipeline is rigid (Cheng and Liu, 1986; Magda, 1997). That is, there is no flow through the pipeline wall because the pipeline is assumed to be an elastic impermeable material. As a result, the pore gradient on the surface of the pipeline should vanish:

$$\frac{\partial p}{\partial n} = 0 \quad \text{at} \quad r = \sqrt{(x-x_0)^2 + (z-z_0)^2} = \frac{D}{2} \tag{32}$$

where x_0 and z_0 denote the coordinates of the centre of the pipeline and n is the normal direction to the surface of the pipeline; D is the pipeline diameter.

5. Numerical results and discussion

In this study, the two-dimensional wave–seabed–pipeline interaction problem can be estimated by finite element model. It can be discretized into unstructured Lagrange-linear elements with a minimum global element size of 0.5 m. The element number $N=5242$ is an appropriate mesh for numerical examples. The time step was 0.01 and the relative tolerance is 0.01. The effects of several important parameters, including the wave depth, wave height, permeability, degree of saturation and wave period, on the wave-induced pore pressure and effective vertical stress, will be investigated. Further, the transient liquefaction in a multilayer seabed based on the excess pore pressure criterion is also discussed.

5.1. Verification of the present model

First, to check the numerical method, the profile of cnoidal wave is compared with the numerical result and experiment data of Chang et al. (2005) in Fig. 2. The cnoidal wave conditions for laboratory experiments are: the wave period $T=2.0$ s; the wave steepness $H/d=0.15$; the water depth $d=24.0$ cm; the wavelength $L=2.97$ m. The free surface elevation of the cnoidal waves was measured by using wave gauge located at $x=4.8$ m (x is the location of wave number at rest) from the location of the wave maker. In the figure, "□" denotes the numerical data from Chang et al. (2005), and "○" is the experimental data from Chang et al. (2005), the solid line represents the present result. As shown in Fig. 2, although some differences between the present model and experimental data are observed, the present result by the numerical simulation reasonably agrees with the experimental data.

Most previous theoretical investigations have focused commonly on the Stokes wave induced seabed response. To check the numerical method, we compare our present result with Gao's previous numerical result, which uses the same boundary condition and Stokes theory. On the other hand, the experimental results by Sudhan et al. (2002) and Turcotte et al. (1984) are also shown in Fig. 3. The main parameters of seabed, pipeline and wave loading are buried depth $e=0.18$ m; pipeline diameter $D=0.2$ m; seabed thickness $h=0.6$ m; water depth $d=0.7$ m; wavelength $L=4.865$ m; wave height $H=0.0938$ m; seabed permeability $k_z=8.1\times10^{-4}$ m/s; shear modulus $G=1.92\times10^{7}$ Pa; Poisson's ratio $\nu=0.25$. Fig. 3 indicates that the numerical results agree overall with the experimental data. Some difference occurs between our present result and Gao's numerical result, which is because we use u–p model with buried pipeline and Gao used Biot consolidation model with trenched pipeline.

5.2. Comparison with the cnoidal wave and Stokes wave

With the parameters of seabed and wave given in Table 1, comparison with the cnodial wave and stokes wave induced seabed response is demonstrated here. The physical variables in the following figures are non-dimensionalized with respect to the amplitude of wave pressure $P_0=\rho_w g H$.

Soil permeability has been recognized as a dominant factor in analyzing the wave-induced seabed response. The vertical distribution of maximum pore pressure P/P_0 and vertical effective stress σ'_{zz}/P_0 for various soil permeability ($k_z=1\times10^{-1}, 1\times10^{-2}, 1\times10^{-3}, 1\times10^{-4}$ m/s) are presented in Fig. 4. In here, the typical value of permeability is taken as 1×10^{-1} m/s for gravel, 1×10^{-2} m/s for coarse sand, 1×10^{-3} m/s for medium fine sand, and 1×10^{-4} m/s for fine sand. As shown in Fig. 4a, the pore pressure p/P_0 for 1×10^{-1} m/s (gravel) indicates a relatively slow decrease versus soil depth, and with more increase in pore pressure at $k_z=1\times10^{-2}$ m/s (coarse sand). For the case with $k_z=1\times10^{-4}$ m/s (fine sand), pore pressure attenuates very rapidly near the seabed surface, where a minimum value is reached. Then, decreases again as depth increases further. For the vertical effective stress σ'_{zz}/P_0, it increases with soil depth increase in the region near the seabed surface in Fig. 4b. It

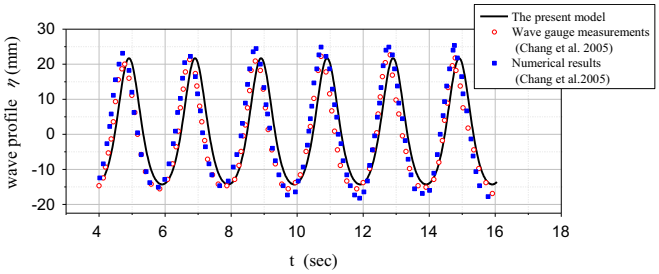

Fig. 2. Comparisons of the free surface profile between the present result and Chang et al. (2005).

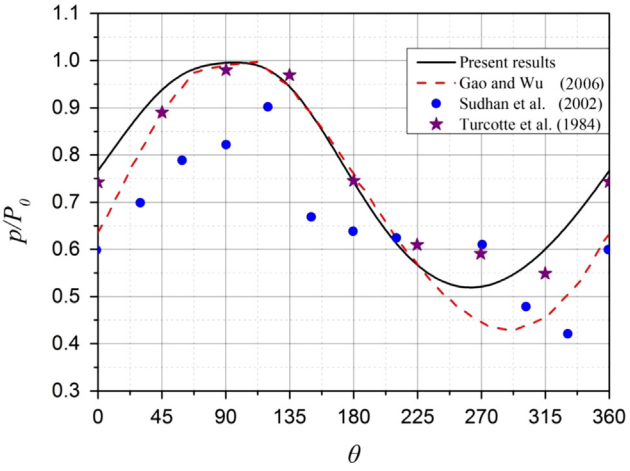

Fig. 3. Verification of numerical model with Gao and Wu (2006), the experimental result by Sudhan et al. (2002) and Turcotte et al. (1984).

reaches a maximum value at a z, then decreases as z increase further. All curves of the cnoidal wave and Stokes wave display similar trends. The solutions of cnoidal wave are obviously greater than that of Stokes wave. For example, the difference between the maximum vertical effective stress induced by cnoidal wave and Stokes wave may reach 70% (Fig. 4b).

Fig. 5 illustrates a comparison between cnoidal wave and Stokes wave with different degrees of saturation (S_r=1.0, 0.98, 0.96, 0.94). As shown in the figure, the degress of saturation significantly affects the wave-induced pore pressure and vertical effective stress. The pore pressure p/P_0 increases as the degree of saturation S_r increases, while the vertical effective stress σ'_{zz}/P_0 decreases as S_r increases. The solutions of cnoidal wave is obviously greater than that of Stokes wave. For example, the difference between the maximum pore pressure induced by cnoidal wave and Stokes wave may reach 65% (Fig. 5a).

Table 1
Input data of water and seabed.

Wave characteristics			
Wave height (H)	1.5 (m)	Water depth (d)	5 (m)
Wave period (T)	8 (s)	Wave Length (L)	56.65 (m)
Water characteristics			
Density (ρ_w)	1025 (kg/m^3)	Modulus of volume (k_w)	2×10^9 (N/m^2)
Seabed characteristics			
Seabed thickness (h)	60 (m)	Density (ρ_s)	2650 (kg/m^3)
Seabed length (l)	100 (m)	Shear modulus (G)	1.92×10^7 (Pa)
Poisson ratio (ν)	0.25	Permeability (k_z)	0.01(m/s)
Porosity (n)	0.4	Degree of saturation (S_r)	0.98

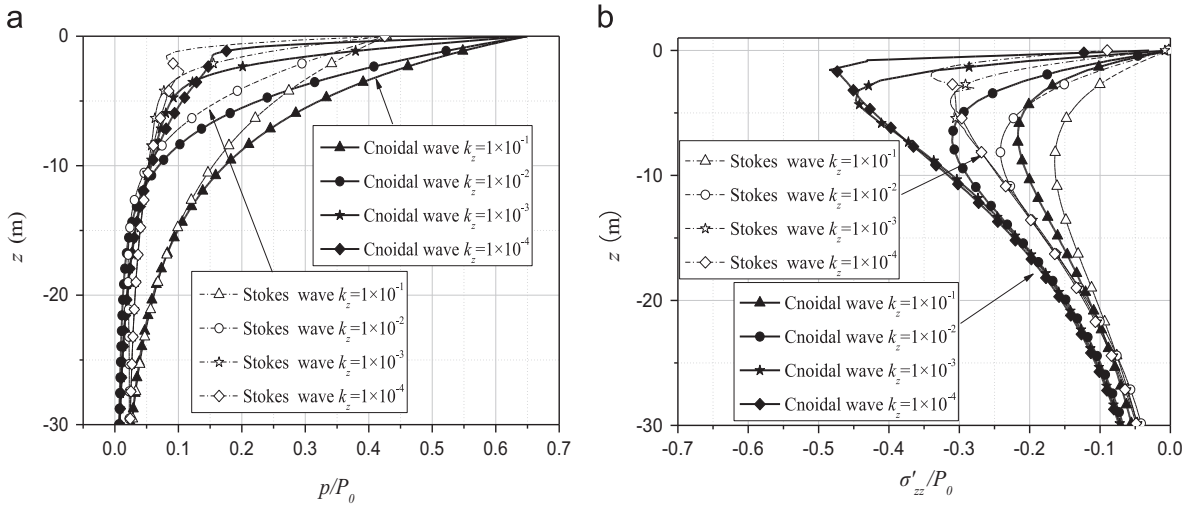

Fig. 4. Distribution of pore pressure and vertical effective stress along depth z for various soil permeability ($k_z=1\times10^{-1}$, 1×10^{-2}, 1×10^{-3}, 1×10^{-4} m/s). (a) p/P_0 along depth z and (b) σ'_{zz}/P_0 along depth z.

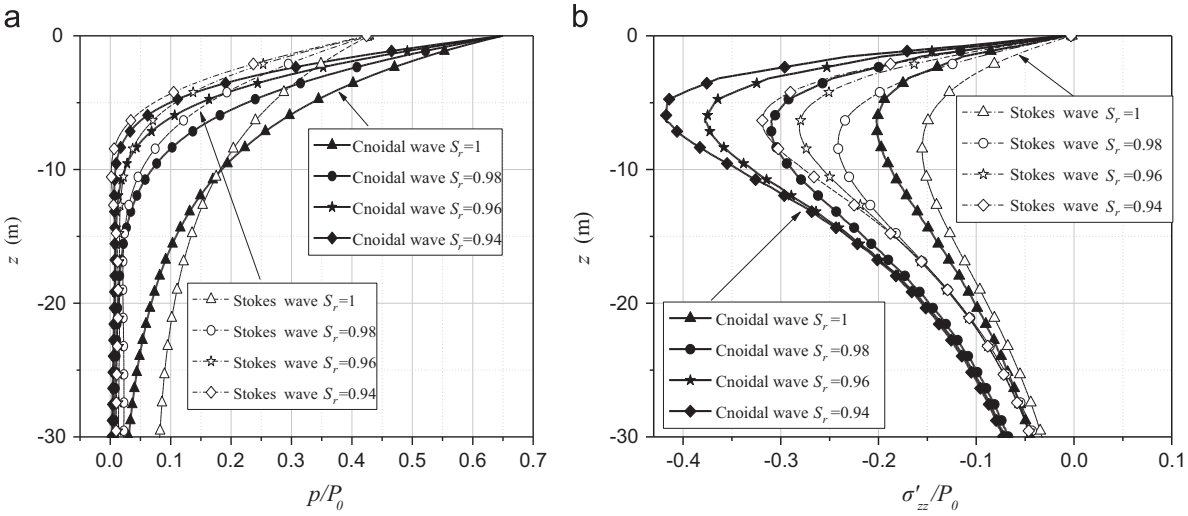

Fig. 5. Distribution of pore pressure and vertical effective stress along depth z for different degrees of saturation (S_r=1.0, 0.98, 0.96, 0.94). (a) p/P_0 along depth z and (b) σ'_{zz}/P_0 along depth z.

5.3. Effect of relative water depth d/L

With the parameters of the seabed, pipeline and wave given in Table 2, the other parameters are wave period $T=8$ s; wave height $H=4.0$ m; pipeline buried depth $e=2$ m. Considering a three-layered seabed: $S_{r1}=1.0$, $S_{r2}=0.97$, $S_{r3}=0.94$; $k_{z1}=0.1$, $k_{z2}=0.01$, $k_{z3}=0.001$ m/s, the vertical and periphery distributions of maximum pore pressure and vertical effective stress for various relative water depths d/L ($d/L=0.084$, 0.116, 0.156) are presented in Fig. 6.

As shown in Fig. 6, the cnoidal wave-induced maximum pore pressure p/P_0 has a slight decrease in the region of the pipeline

Table 2
Input data of standard case for parametric study.

Water characteristics			
Density (ρ_w)	1025 (kg/m^3)	Modulus of volume (k_w)	2×10^9 (N/m^2)
Seabed characteristics			
Seabed thickness (h_1, h_2, h_3)	20 (m)	Density (ρ_{s1}, ρ_{s2}, ρ_{s3})	2650(kg/m^3)
Seabed length (l)	100 (m)	Shear modulus (G_1, G_2, G_3)	1.92×10^7 (Pa)
Poisson ratio (ν_1, ν_2, ν_3)	0.25	Porosity (n_1, n_2, n_3)	0.4
Pipeline characteristics			
Young's modulus (E_p)	6.8×10^{10} (N/m^2)	Density (ρ_p)	2700 (kg/m^3)
Pipeline thickness (t_p)	0.1 (m)	Pipeline outer diameter (D)	2 (m)
Poisson ratio (ν_p)	0.32		

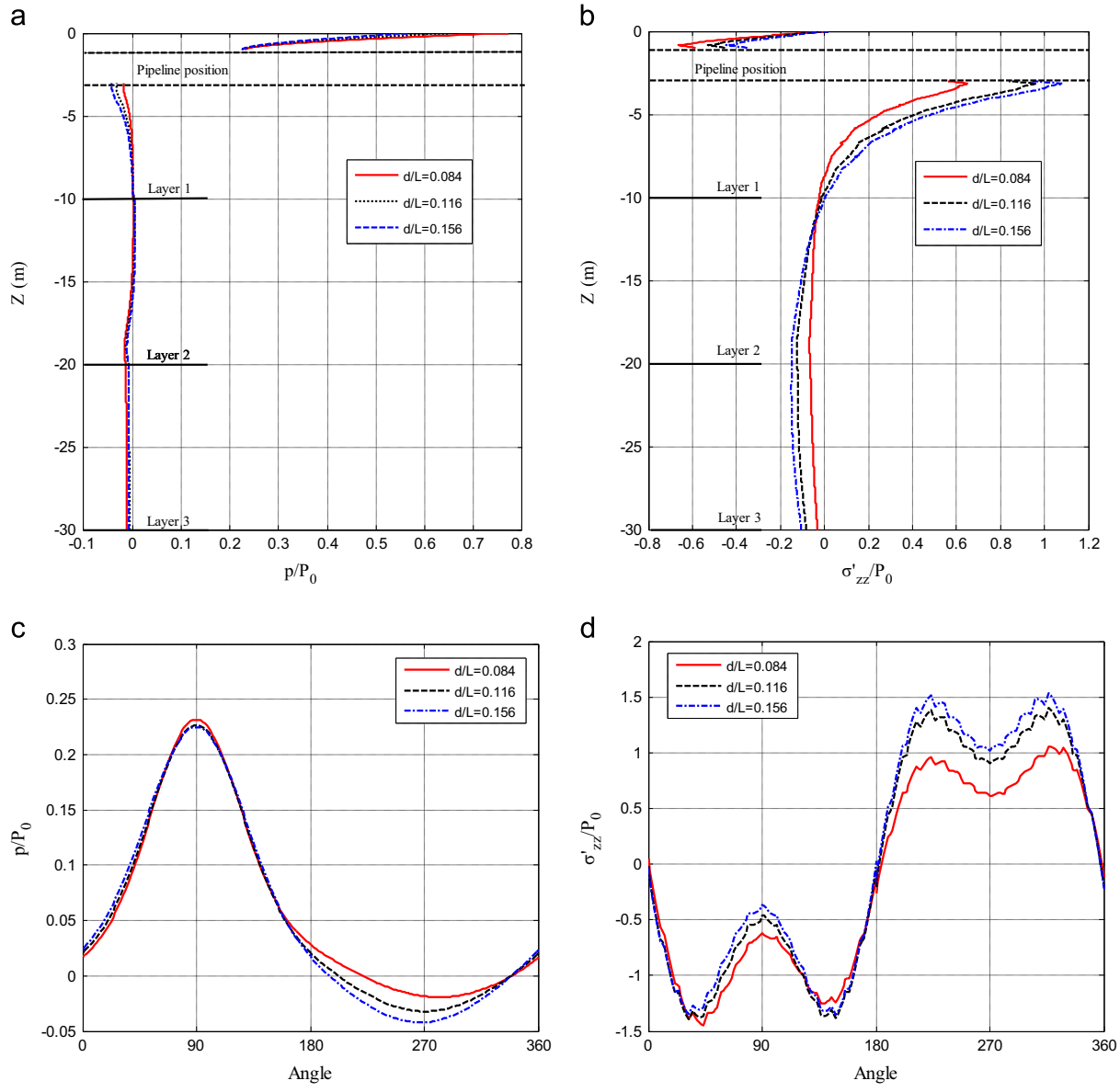

Fig. 6. Distribution of pore pressure and vertical effective stress for various relative water depths ($d/L=0.084$, 0.116, 0.156). (a) p/P_0along depth z. (b) σ'_{zz}/P_0 along depth z. (c) p/P_0 along the periphery of pipeline and (d) σ'_{zz}/P_0 along the periphery of pipeline.

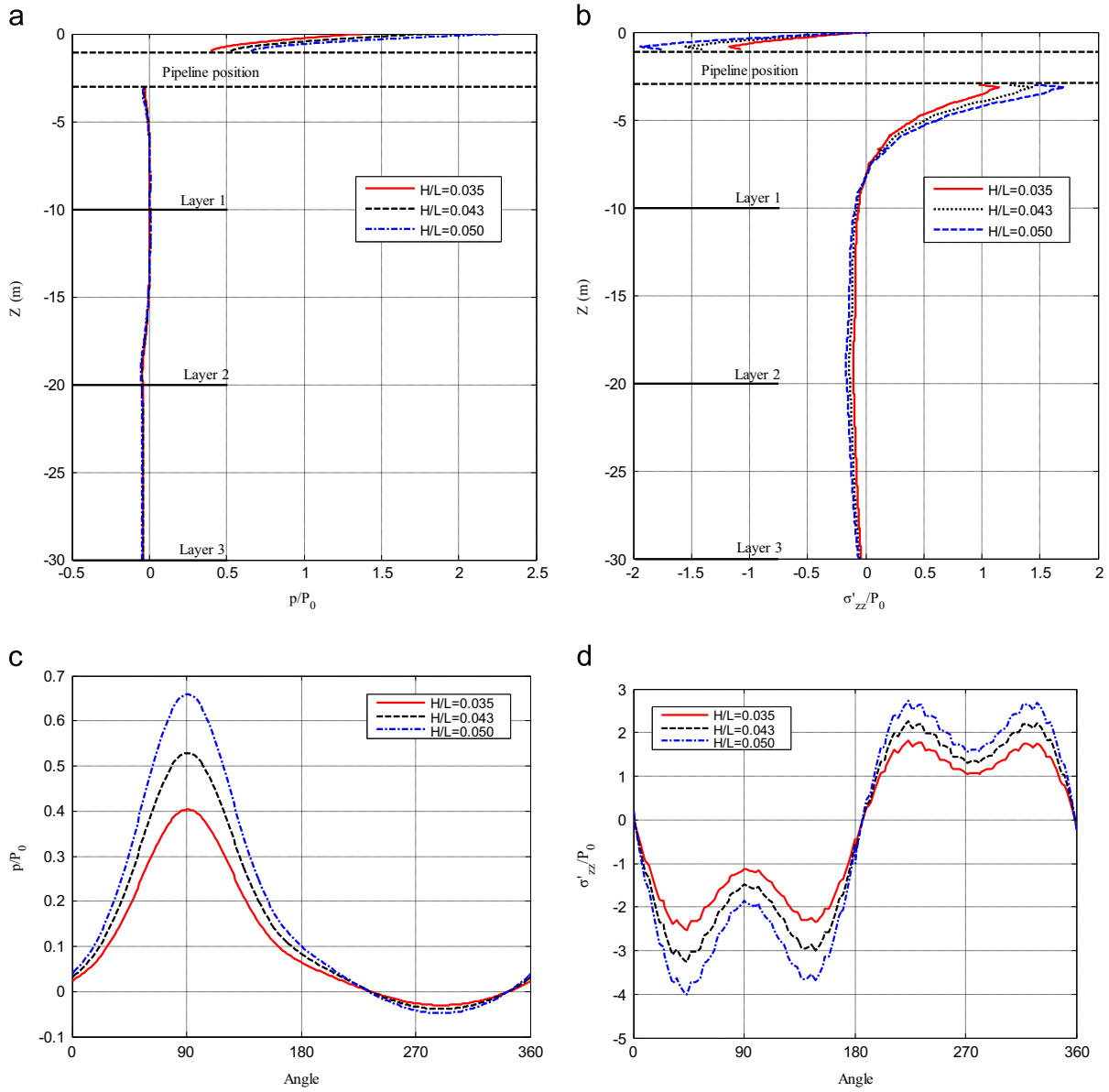

Fig. 7. Distribution of pore pressure and vertical effective stress for various wave steepnesses (H/L= 0.035, 0.043, 0.050). (a) p/P_0 along depth z and (b) σ'_{zz}/P_0 along depth z. (c) p/P_0 along the periphery of pipeline and (d) σ'_{zz}/P_0 along the periphery of pipeline.

when the relative water depth d/L increases (Fig. 6a). The maximum vertical effective stress σ'_{zz}/P_0 increases when the relative water depth d/L increases (Fig. 6b). Fig. 6c shows that the maximum pore pressure p/P_0 along the periphery of the pipeline has an obvious increase when the relative water depth d/L increases at the bottom of the pipeline (θ=270°); however, this variation is not obvious at the top of pipeline. The distribution of vertical effective stress σ'_{zz}/P_0 along the periphery of the pipeline evidently increases when the relative water depth d/L increases. This implies that the influence of the relative water depth on the vertical effective stress is more obvious than the effect of the pore pressure, especially in the location along the periphery of the pipeline.

5.4. *Effective of wave steepness H/L*

Fig. 7 illustrates the distributions of maximum pore pressure p/P_0 and vertical effective stress σ'_{zz}/P_0 for three wave steepnesses H/L=0.035, 0.043, 0.050. Based on input data presented in Table 2, the other parameters are wave period T=8 s; water depth d=5.0 m; pipeline buried depth e=2 m. For the three-layered seabed considered: S_{r1}=1.0, S_{r2}=0.97, S_{r3}=0.94; k_{z1}=0.1, k_{z2}=0.01, k_{z3}=0.001 m/s.

The influence of the wave steepness on the maximum pore pressure p/P_0 along seabed depth z is rather insignificant (Fig. 7a). However, the maximum vertical effective stress σ'_{zz}/P_0 near the pipeline increases when the relative wave height H/L increases (Fig. 7b). Fig. 7c and d indicates that the maximum pore pressure p/P_0 and vertical effective stress σ'_{zz}/P_0 along the periphery of the pipeline have obviously increased when the wave steepness H/L increases. The maximum value occurs at the top of the pipeline. For example, the maximum value of pore pressure along the periphery of the pipeline is 0.4 when H/L=0.035, and rises to 0.65 when H/L=0.050. The maximum value of vertical effective stress is 2.4 when H/L=0.035, and reaches 4.0 when H/L=0.050. It is worth noting that the wave steepness affects the cnoidal wave-

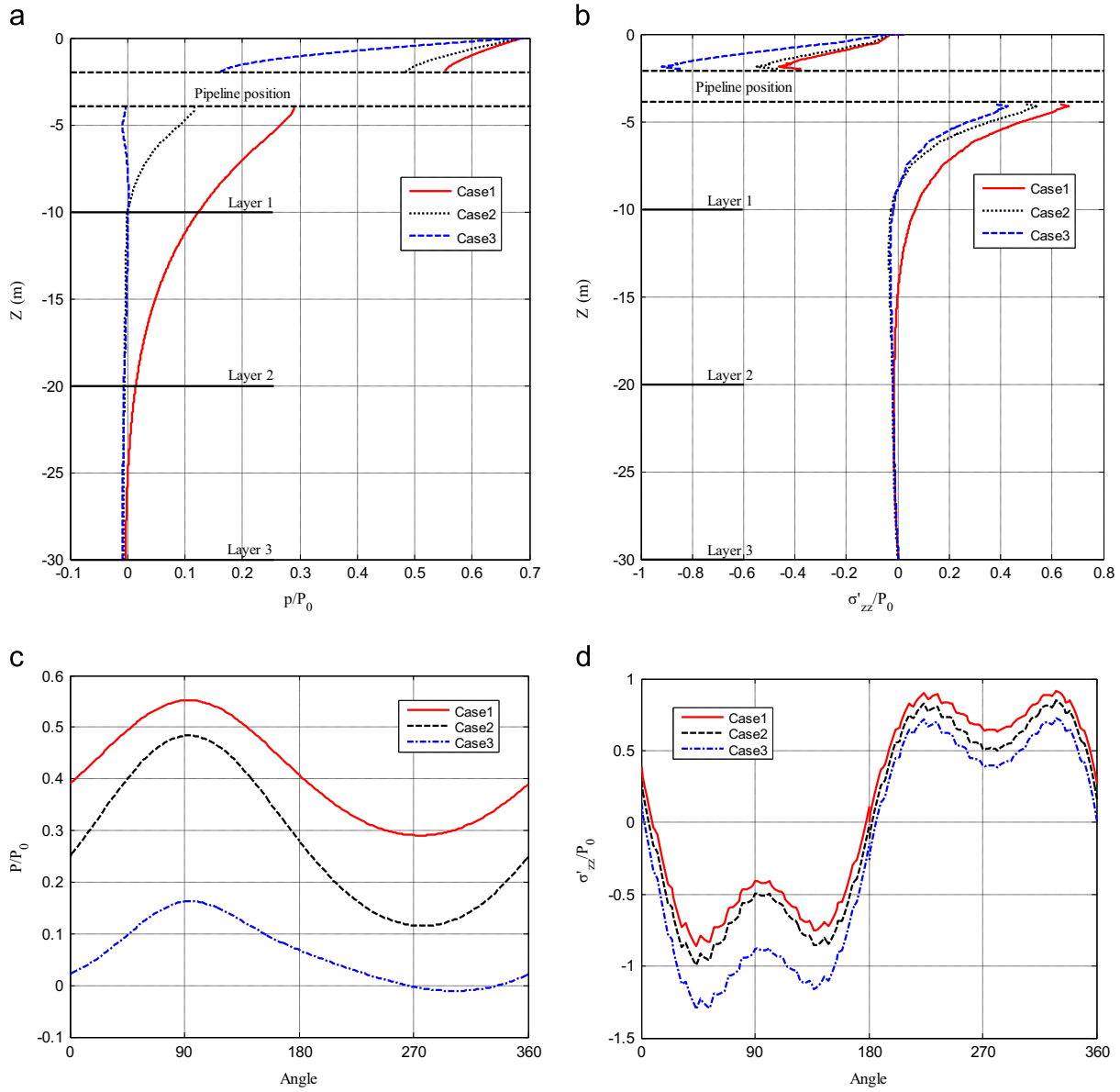

Fig. 8. Distribution of pore pressure and vertical effective stress for a single-layered seabed (Case 1: $k_{z1}=k_{z2}=k_{z3}=0.1$ m/s); a two-layered seabed (Case 2: $k_{z1}=k_{z2}=0.1$ m/s, $k_{z3}=0.001$ m/s); and a three-layered seabed (Case 3: $k_{z1}=0.1$ m/s, $k_{z2}=0.01$ m/s, $k_{z3}=0.001$ m/s). (a) p/P_0 along depth z and (b) σ'_{zz}/P_0 along depth z. (c) p/P_0 along the periphery of pipeline and (d) σ'_{zz}/P_0 along the periphery of pipeline.

induced soil response obviously along the periphery of the pipeline.

5.5. *Effect of soil permeability*

Consider a seabed with three kinds of case, a single-layered seabed (Case 1: $k_{z1}=k_{z2}=k_{z3}=0.1$ m/s); a two-layered seabed (Case 2: $k_{z1}=k_{z2}=0.1$ m/s, $k_{z3}=0.001$ m/s); and a three-layered seabed (Case 3: $k_{z1}=0.1$ m/s, $k_{z2}=0.01$ m/s, $k_{z3}=0.001$ m/s). The wave and seabed parameters are wave period $T=8$ s, wave height $H=2$ m, water depth $d=5$ m, pipeline buried depth $e=3$ m, degree of saturation of three-layered seabed $S_{r1}=S_{r2}=S_{r3}=0.98$. The other parameters are listed in Table 2.

Fig. 8 shows that the differences between the three cases are significant. For example, as shown in Fig. 8a, for coarse sand used as the seabed (Case 1), the maximum pore pressure p/P_0 attenuates very slowly along depth z. For three-layered sand (Cases 3), the pore pressure p/P_0 attenuates very rapidly. The maximum vertical effective stress σ'_{zz}/P_0 decreases when the soil permeability of the lower layer decreases (Fig. 8b). From the results presented in Fig. 8a, the surface layer is gravel ($k_{z1}=0.1$ m/s), while the lower floor is coarse or intermediate sand (Case 2, Case 3), and in these cases, the pore pressure along seabed depth z attenuates faster than the single-layered seabed (Case 1). The reduction in pore pressure p/P_0 is attributed to the damping by the lower layer with a soil of much smaller permeability than the top layer. This is because the lower permeability coarse or intermediate sand has lower fluid velocity to transmit through the voids between grains than the higher permeability seabed with gravel. The vertical effective stress along the seabed depth first increases, where a maximum value is reached. Then, the vertical effective stress decreases as z increases further (Fig. 8b).

As shown in Fig. 8c and d, the pore pressure p/P_0 in Case 1 is greater than that in Case 2 and Case 3. The pore pressure decreases and vertical effective stress increases when the soil permeability of the lower layer decreases. For instance, the

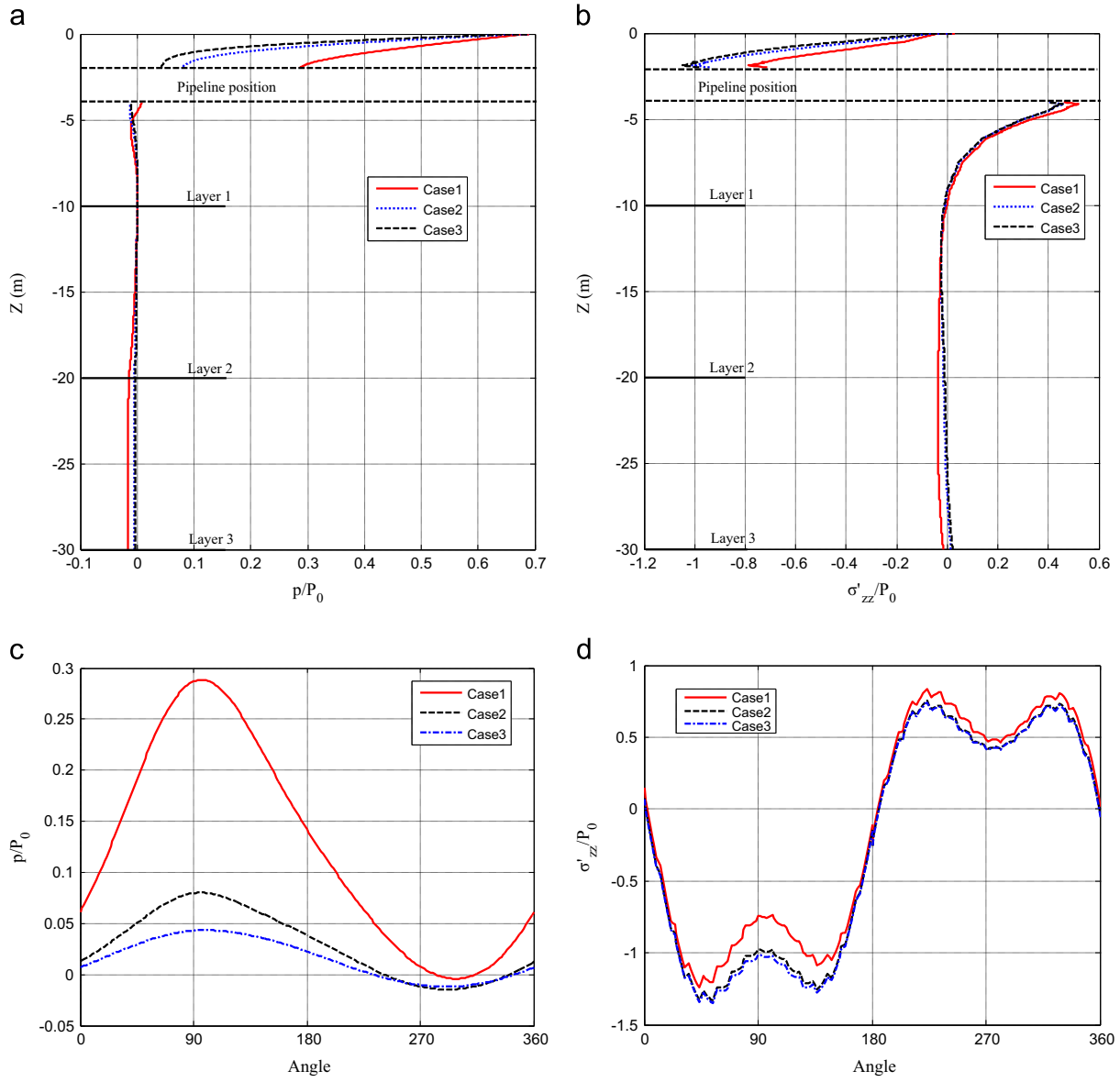

Fig. 9. Distribution of pore pressure and vertical effective stress for various degrees of saturation: Case 1: $S_{r1}=S_{r2}=S_{r3}=0.99$; Case 2: $S_{r1}=0.99$, $S_{r2}=S_{r3}=0.96$; Case3: $S_{r1}=0.99$, $S_{r2}=0.96$, $S_{r3}=0.93$. (a) p/P_0 along depth z and (b) σ'_{zz}/P_0 along depth z. (c) p/P_0 along the periphery of pipeline and (d) σ'_{zz}/P_0 along the periphery of pipeline.

maximum pore pressure in Case 1 is three times that in Case 3, and the maximum effective vertical stress in Case 3 is two times that in Case 1.

5.6. Effect of the degree of saturation

Based on the same parameters as in Section 5.5, Fig. 9 illustrates the maximum pore pressure p/P_0 and vertical effective stress σ'_{zz}/P_0 for the three cases: Case 1: $S_{r1}=S_{r2}=S_{r3}=0.99$; Case 2: $S_{r1}=0.99$, $S_{r2}=S_{r3}=0.96$; Case 3: $S_{r1}=0.99$, $S_{r2}=0.96$, $S_{r3}=0.93$. As shown in Fig. 9a and b, the amplitude of pore pressure p/P_0 in the seabed decreases as the degree of saturation within the lower layer decreases, while the vertical effective stress σ'_{zz}/P_0 increases as the degree of saturation within the lower layer decreases. Fig. 9c indicates that the pore pressure p/P_0 along the periphery of the pipeline decreases obviously when the degree of saturation within the lower layer decreases. For instance, the maximum value of pore pressure along the periphery of the pipeline is 0.29 in Case 1, and reduces to 0.049 in Case 3. The maximum pore pressure in Case 1 is six times that in Case 3. The vertical effective stress σ'_{zz}/P_0 along the periphery of the pipeline increases as the degree of saturation decreases within the lower layer.

5.7. Effect of the period T

In general, the wave period T will play an important role in simulation of the wave pressure of cnoidal wave. Fig. 10 shows that the maximum distribution of pore pressure p/P_0 and vertical effective stress σ'_{zz}/P_0 vary with the different wave periods $T=8$, 10, 12 s. As shown in Fig. 10a, the pore pressure p/P_0 slightly decreases as the wave period T increases. The vertical effective stress σ'_{zz}/P_0 increases as the wave period T increases (Fig. 10b). Fig. 10c and d shows that the pore pressure increases and the vertical effective stress decreases along the periphery of the pipeline when the wave period T increases.

As shown in Fig. 11, the shapes of troughs of pore pressure become longer and flatter when the wave period T increases. The

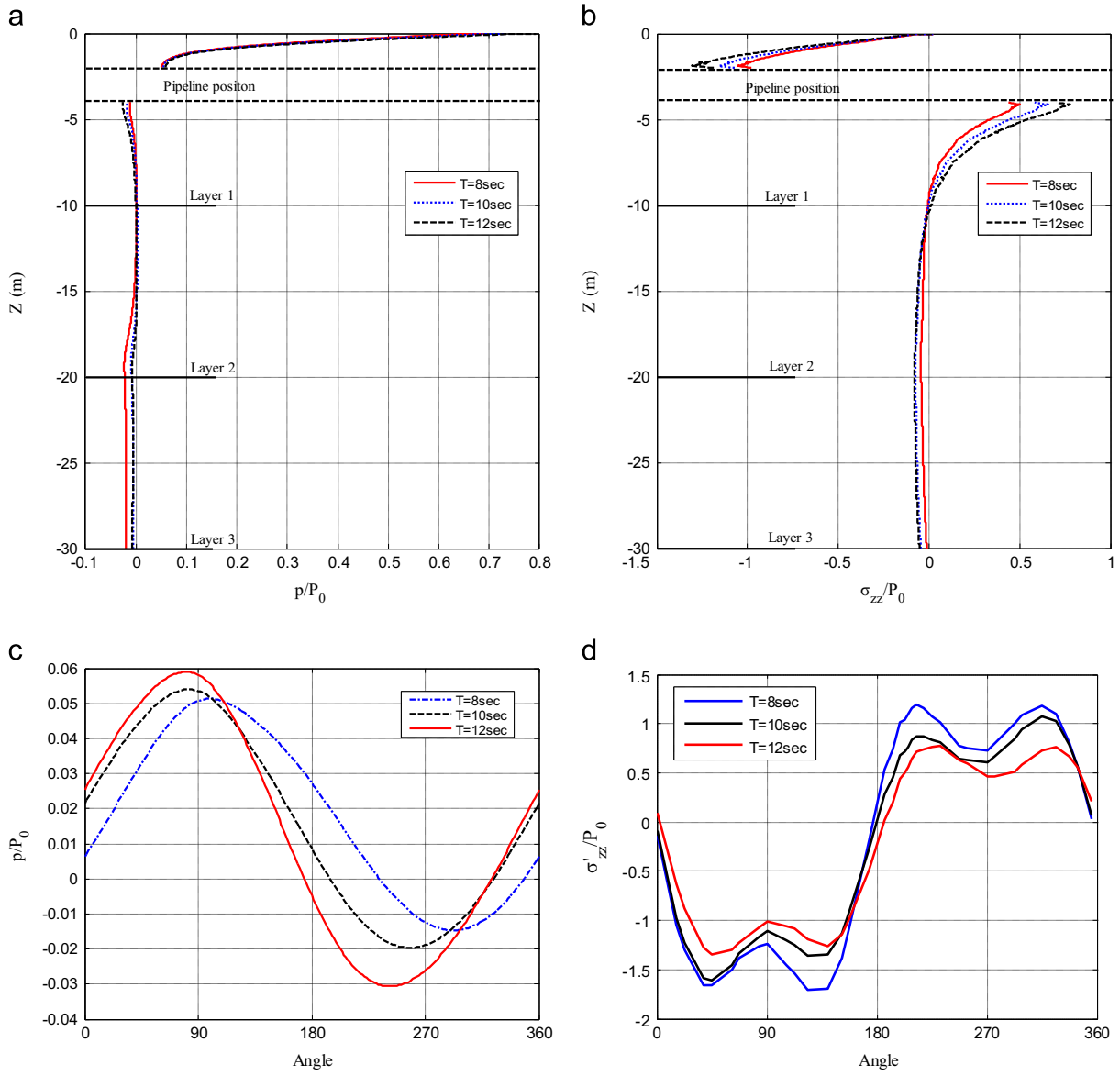

Fig. 10. Distribution of pore pressure and vertical effective stress for various wave periods (T=8, 10, 12 s). (a) p/P_0 along depth z and (b) σ'_{zz}/P_0 along depth z. (c) p/P_0 along the periphery of pipeline and (d) σ'_{zz}/P_0 along the periphery of pipeline.

maximum value of pore pressure p/P_0 increases when the wave period T increases. For example, the maximum value of pore pressure is 0.61 at the wave period T=6 s, and rises to 0.80 at the wave period T=12 s. Fig. 11b indicates that the maximum of vertical effective stress σ'_{zz}/P_0 increases when the wave period T increases. For example, the maximum value of vertical effective stress σ'_{zz}/P_0 is 0.85 at the wave period T=6 s, and reaches 1.75 at the wave period T=12 s.

5.8. Transient liquefaction under cnoidal wave

The wave-induced excess pore pressure may lead to transient liquefaction. The criterion of liquefaction used for a 2D wave, which is suggested by Zen and Yamazaki (1993) is as follows:

$$-(\gamma_s-\gamma_w)z+[P_b(x,t)-p(x,z,t)]\le 0 \tag{33}$$

where γ_s is the unit weight of the seabed; γ_w is the unit weight of water; P_b is the pore pressure on the mudline (z=0); p is the field of pore pressure in the seabed.

This equation indicates that transient liquefaction may occur when its excess pore pressure becomes greater than the overburden soil pressure. So, the excess pore pressure is the key factor in estimating the transient liquefaction.

It was stated that the cnoidal wave-induced seabed response is affected significantly by the soil permeability and degree of saturation, as discussed in Sections 5.5–5.6. Therefore, it is necessary to examine further its influence on the liquefaction phenomenon. The input data is tabulated in Table 3.

In the examples presented in Fig. 12, it is observed that the liquefaction depth and region increase as the soil permeability k_z decreases. It is also found that liquefaction always occurs in a seabed with soil permeability $k_{z1}\le 1\times 10^{-3}$ m/s, while liquefaction does not occur at $k_{z1}=5\times 10^{-3}$ m/s in this case. For example, the maximum liquefied depth z is about 0.5 m for $k_{z1}=1\times 10^{-3}$ m/s, and reaches 1.5 m for $k_{z1}=1\times 10^{-5}$ m/s. This implies that lower permeability has a greater liquefaction potential than higher permeability under the same condition.

The distribution of liquefaction versus the degree of saturation (S_r) is presented in Fig. 13. Generally speaking, the liquefied depth

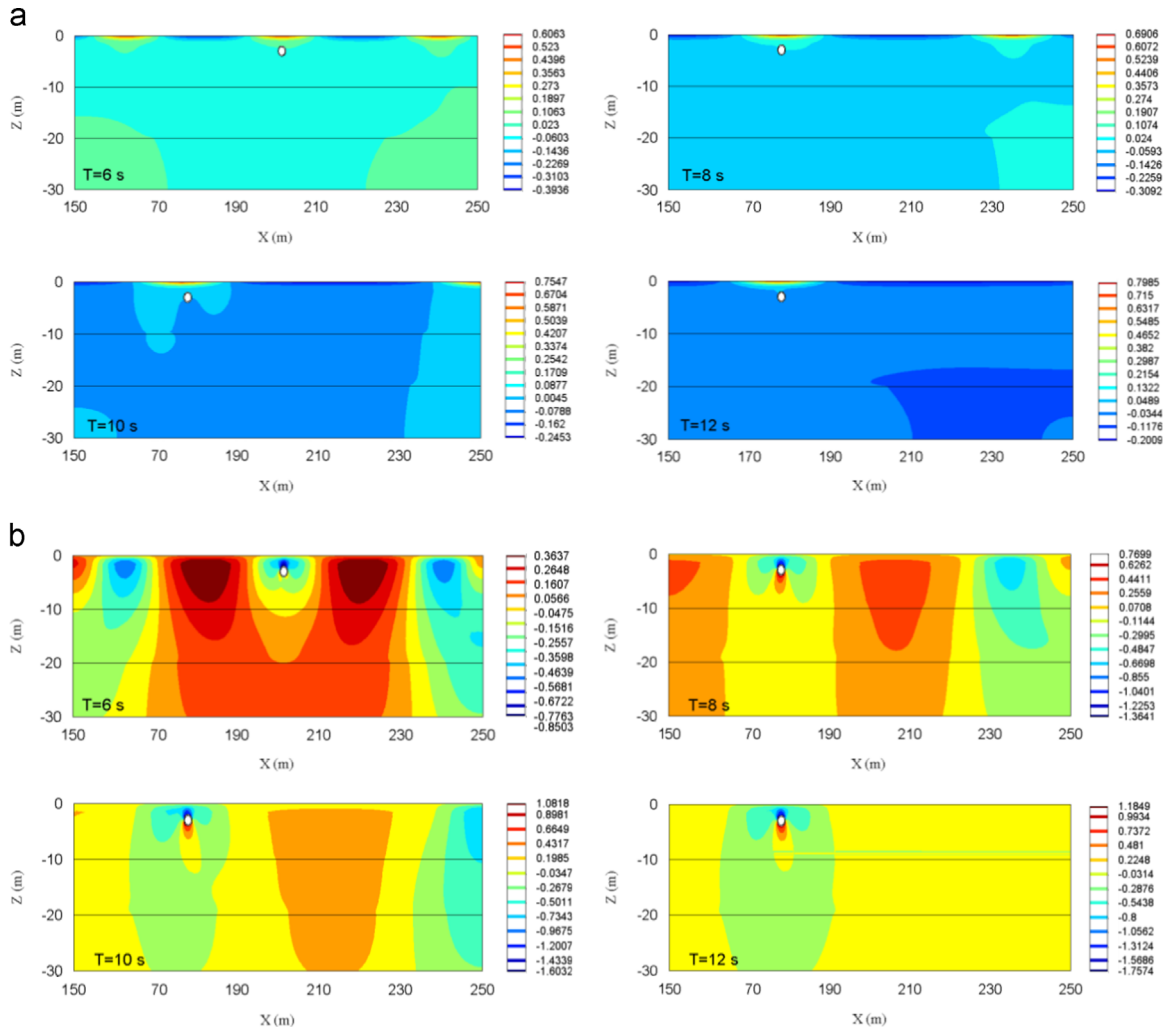

Fig. 11. Contour of pore pressure and vertical effective stress along depth z for various wave periods (T=6, 8, 10, 12 s). (a) p/P_0 along seabed depth z and (b) σ'_{zz}/P_0 along seabed depth z.

Table 3
Input data of standard case for parametric study.

Wave characteristics			
Wave height (H)	2 (m)	Water depth (d)	5 (m)
Wave period (T)	8 (s)	Wave Length (L)	56.65 (m)
Water characteristics			
Density (ρ_w)	1025 (kg/m^3)	Modulus of volume (k_w)	2×10^9 (N/m^2)
Seabed characteristics			
Seabed thickness (h_1, h_2, h_3)	10 (m)	Density (ρ_{s1}, ρ_{s2}, ρ_{s3})	1400 (kg/m^3)
Seabed Length (l)	100 (m)	Shear modulus (G_1, G_2, G_3)	1.92×10^7 (Pa)
Poisson ratio (ν_1, ν_2, ν_3)	0.25	Permeability (k_{z1}, k_{z2}, k_{z3})	7×10^{-3}, 7×10^{-3}, 7×10^{-3} (m/s)
Porosity (n_1, n_2, n_3)	0.4	Degree of saturation (S_{r1}, S_{r2}, S_{r3})	0.96
Pipeline characteristics			
Young's modulus (E_p)	6.8×10^{10} (N/m^2)	Density (ρ_p)	2700 (kg/m^3)
Pipeline thickness (t_p)	0.1 (m)	Pipeline outer diameter (D)	2 (m)
Poisson ratio (ν_p)	0.32	Buried depth of pipeline (e)	2(m)

z increases as the degree of saturation S_r decreases. For example, the liquefied depth z=0.7 m for S_r=0.98, and reaches 1.5 m for S_r=0.90. It is worth noting that no liquefaction occurs in a saturated seabed (S_r=1.0).

At least from the numerical examples presented in Figs. 12 and 13, putting a gravel or coarse sand with high permeability on top of the seabed may serve to reduce the liquefaction potential. On the other hand, modifying the degree of saturation of the soil can also reduce or inhibit liquefaction in a porous seabed.

6. Conclusion

In this study, a numerical model is developed to investigate the complicated problem of wave–seabed–pipeline interaction. The

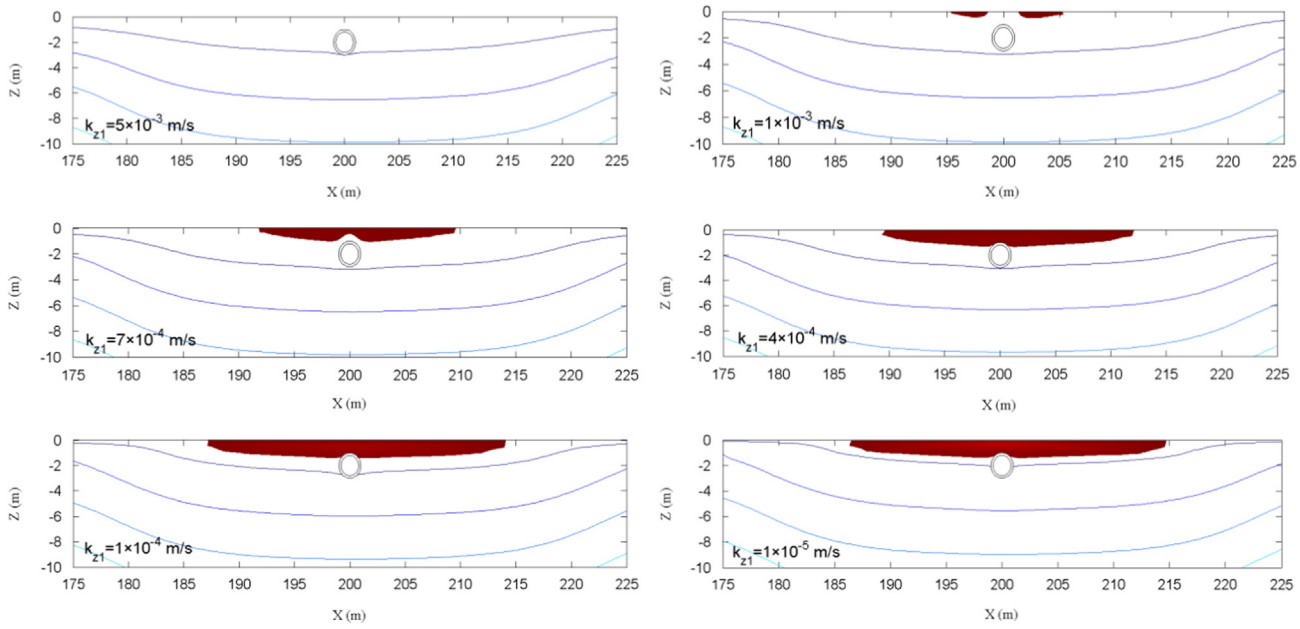

Fig. 12. Liquefaction depth for different soil permeability k_{z1}.

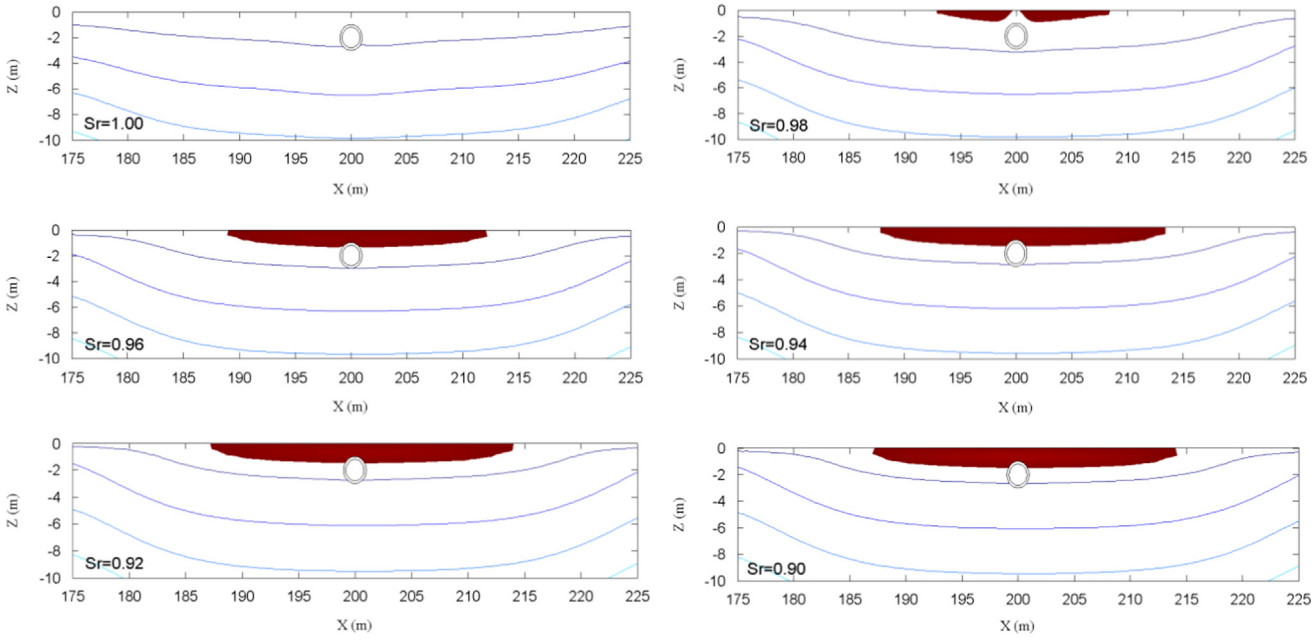

Fig. 13. Liquefaction depth for different degrees of saturation S_r.

cnoidal wave theory can be solved by using Taylor series expansion and the precise integration method. The seabed is treated as a porous medium and characterized by Biot's theory (u–p model). The effects of wave and seabed characteristics on the seabed response within the seabed and around the pipeline circumference are investigated. Based on the numerical results, the following conclusions can be drawn:

(1) The soil permeability is an important concern in seabed response. The pore pressure p/P_0 for $k_z=1\times10^{-1}$ m/s (gravel) indicates a relatively slow decrease versus soil depth, and for $k_z=1\times10^{-4}$ m/s (fine sand), pore pressure attenuates very rapidly near the seabed surface.

(2) The degree of saturation is another important parameter in determining the seabed response. The pore pressure p/P_0 increases and the vertical effective stress σ'_{zz}/P_0 decreases as the degree of saturation S_r increases.

(3) The wave period plays an important role in simulating the wave pressure of a cnoidal wave. The shapes of the troughs of pore pressure become longer and flatter as the wave period increases. The maximum value of pore pressure increases when the wave period increases.

(4) The liquefaction depth and region increase as the soil permeability or the degree of saturation decrease. Putting a gravel or coarse sand with high permeability on top of the seabed may serve to reduce the liquefaction potential. On the other hand,

modifying the degree of saturation of the soil can also reduce or inhibit liquefaction in a porous seabed.

Acknowledgments

The research was financially supported by the National Natural Science Foundation of China with Grant (Project nos. 41372286 and 41330633). The project was also supported by the State Key Laboratory of Ocean Engineering (Project no. GKZD010059).

Appendix A. Supporting information

Supplementary data associated with this article can be found in the online version at http://dx.doi.org/10.1016/j.oceaneng.2015.04.032.

References

Biot, M.A., 1956. Theory of propagation of elastic waves in a fluid-saturated porous solid. I. Low frequency range. J. Acoust. Soc. Am. 28, 168–178.
Biot, M.A., 1962. Mechanics of deformation and acoustic propagation in porous media. J. Appl. Phys. 33, 1482–1498.
Cai, Y.Q., Sun, H.L., Xu, C.J., 2007. Steady state responses of poroelastic half-space soil medium to a moving rectangular load. Int. J. Solids Struct. 44, 7183–7196.
Chang, K.A., Hsu, T.J., Liu, P.L.F., 2005. Vortex generation and evolution in water waves propagating over a submerged rectangular obstacle. Part II: Cnoidal waves. Coast. Eng. 52, 257–283.
Cheng, A.H.D., Liu, P.L.F., 1986. Seepage force on a pipeline buried in a poroelastic seabed under wave loading. Appl. Ocean Res. 8 (1), 22–32.
Cho, Y.S., 2003. A note on estimation of the Jacobian elliptic parameter in cnoidal wave theory. Ocean. Eng. 30, 1915–1922.
Fenton, J.D., 1990. Nonlinear wave theories. In: Le Méhauté, B., Hanes, D.M. (Eds.), The Sea, vol. 9: Ocean Engineering Science. Wiley, New York, pp. 3–25.
Fenton, J.D., Gardiner-Garden, R.S., 1982. Rapidly-convergent methods for evaluating elliptic integrals and theta and elliptic functions. J. Aust. Math. Soc. Ser. B 24 (01), 47–58.
Gao, F.P., Gu, X.Y., Jeng, D.S., Teo, H.T., 2002. An experimental study for wave-induced instability of pipelines: the breakout of pipelines. Appl. Ocean Res. 24 (2), 83–90.
Gao, F.P., Han, X.T., Cao, J., Sha, Y., Cui, J.S., 2012. Submarine pipeline lateral instability on a sloping sandy seabed. Ocean. Eng. 50 (15), 44–52.
Gao, F.P., Wu, Y.X., 2006. Non-linear wave induced transient response of soil around a trenched pipeline. Ocean. Eng. 33, 311–330.
Gao, F.P., Yan, S.M., Yang, B., Luo, C.C., 2011. Steady flow-induced instability of a partially embedded pipeline: pipe–soil interaction mechanism. Ocean. Eng. 38 (7), 934–942.
Hedges, T.S., 1995. Regions of validity of analytical wave theories. Proc. Inst. Civ. Eng. Water, Marit Energy 112 (2), 111–114.
Hsu, J.R.C., Jeng, D.S., 1994. Wave-induced soil response in an unsaturated anisotropic seabed of finite thickness. Int. J. Numer. Anal. Methods Geomech. 18, 785–807.
Hsu, J.R.C., Jeng, D.S., Lee, C.P., 1995. Oscillatory soil response and liquefaction in an unsaturated layered seabed. Int. J. Numer. Anal. Methods Geomech. 19 (12), 825–849.
Isobe, M., 1985. Calculation and application of first-order cnoidal wave theory. Coast. Eng. 9, 309–325.
Jeng, D.S., 2013. Porous Models for Wave–Seabed Interactions. Shanghai Jiaotong University Press and Springer, China, pp. 7–32.
Jeng, D.S., Cha, D.H., 2003. Effects of dynamic soil behaviour and wave non-linearity on the wave-induced pore pressure and effective stresses in porous seabed. Ocean. Eng. 30 (16), 2065–2089.
Jeng, D.S., Cheng, L., 2000. Wave-induced seabed instability around a buried pipe in a poroelastic seabed. Comput. Geotech. 26 (1), 43–64.
Korteweg, D.J., De Vries, G., 1895. On the change of form of long waves advancing in a rectangular canal, and on a new type of long stationary waves. Philos. Mag. 39, 422–443.
Liu, H., Jeng, D.S., 2007. A semi-analytical solution for random wave-induced soil response in marine sediments. Ocean. Eng. 34 (8–9), 1211–1224.
Madsen, O.S., 1978. Wave-induced pore pressures and effective stresses in a porous bed. Géotechnique 28, 377–393.
Magda, W., 1997. Wave-induced uplift force acting on a submarine buried pipeline in a compressible seabed. Ocean. Eng. 24 (6), 551–576.
McDougal, W.G., Davidson, S.H., Monkmeyer, P.L., Sollitt, C.K., 1988. Wave-induced forces on buried pipelines. J. Waterw., Port, Coast., Ocean Eng. 114 (2), 220–263.
Mei, C.C., Foda, M.A., 1981. Wave-induced responses in a fluid-filled poro-elastic solid with a free surface—a boundary layer theory. Geophys. J. R. Astron. Soc. 66, 597–631.
Mei, C.C., Stiassnie, M., Yue, D.K.P., 2005. Theory and Applications of Ocean Surface Waves: Nonlinear Aspects. World Scientific, New York.
Rahman, M.S., El-Zahaby, K., Booker, J., 1994. A semi-analytical method for the wave-induced seabed response. Int. J. Numer. Anal. Methods Geomech. 18, 213–236.
Shabani, B., Jeng, D.S., 2008. 3D modeling of wave–seabed–pipeline in marine environments. Open Civ. Eng. J. 2, 1–22.
Sudhan, C.M., Sundar, V., Rao, S.N., 2002. Wave induced forces around buried pipeline. Ocean Eng. 29, 533–544.
Sumer, B.M., Fredsøe, J., 1991. Onset of scour below a pipeline exposed to waves. Int. J. Offshore Polar Eng. 1 (3), 189–194.
Sumer, B.M., Tuelsen, C., Sichmann, T., Fredsøe, J., 2001. Onset of scour below pipelines and self-buried. Coast. Eng. 42 (4), 213–235.
Synolakis, C.E., Deb, M.K., Skjelbreia, J.E., 1988. The anomalous behavior of the runup of cnoidal waves. Phys. Fluids 31, 3–5.
Turcotte, B.R., Liu, P.L.F., Kulhawy, F.H., 1984. Laboratory Evaluation of Wave Tank Parameters for Wave–Sediment Interaction. School of Civil and Environmental Engineering, Cornell University, Ithaca, New York.
Ulker, M.B.C., Rahman, M.S., 2009. Response of saturated and nearly saturated porous media: different formulations and their applicability. Int. J. Numer. Anal. Methods Geomech. 33 (5), 633–664.
Wang, L.Z., Shi, R.W., Yuan, F., Guo, Z., Yu, L.Q., 2011. Global buckling of pipelines in the vertical plane with a soft seabed. Appl. Ocean Res. 33, 130–136.
Wiegel, R.L., 1960. A presentation of cnoidal wave theory for practical application. J. Fluid Mech. 7 (2), 273–287.
Xu, H.X., Dong, P., 2011. A probabilistic analysis of random wave-induced liquefaction. Ocean Eng. 38, 860–867.
Xu, Y.F., Wang, J.H., Chen, J.J., 2013. Cnoidal water wave induced seepage in a permeable seabed with a defined thickness. Coast. Eng. 80, 95–99.
Xu, Y.F., Xia, X.H., Wang, J.H., 2012. Calculation and approximation of the cnoidal function in cnoidal wave theory. Comput. Fluids 68, 242–247.
Yamamoto, T., Koning, H.L., Sellmeiher, H., Hijum, E.V., 1978. On the response of a poro-elastic bed to water waves. J. Fluid Mech. 87, 193–206.
Ye, J.H., Jeng, D.S., Liu, P.L.F., Chan, A.H.C., Wang, R., Zhu, C.Q., 2014. Breaking wave-induced response of composite breakwater and liquefaction in seabed foundation. Coast. Eng. 85, 72–86.
Yuhi, M., Ishida, H., 1998. Analytical solution for wave-induced seabed response in a soil–water two-phase mixture. Coast. Eng. 40 (4), 367–381.
Zen, K., Yamazaki, H., 1993. Wave-induced liquefaction in a permeable seabed. Rept. Port Harb. Res. Inst. 31, 155–192.
Zhang, J., Zheng, J., Zhang, C., Jeng, D.S., Guo, Y., 2013. Numerical study on the interaction between waves and twin pipelines in sandy seabed. J. Coast. Res. 65, 428–433.
Zhong, W.X., 2004. On precise integration method. J. Comput. Appl. Math. 163, 59–78.
Zhou, X.L., Jeng, D.S., Yan, Y.G., Wang, J.H., 2013. Wave-induced multi-layered seabed response around a buried pipeline. Ocean Eng. 72, 195–208.
Zhou, X.L., Wang, J.H., Zhang, J., Jeng, D.S., 2014. Wave and current induced seabed response around a submarine pipeline in an anisotropic seabed. Ocean Eng. 75, 112–127.
Zhou, X.L., Xu, B., Wang, J.H., Li, Y.L., 2011. An analytical solution for wave-induced seabed response in a multi-layered poro-elastic seabed. Ocean Eng. 38, 119–129.
Zienkiewicz, O.C., Chang, O.C., Bettess, P., 1980. Drained, undrained, consolidating and dynamic behaviour assumptions in soils. Géotechnique 30, 385–395.